49th AIAA Aerospace Sciences Meeting
4-7 January 2011, Orlando, FL

AIAA 2011-1254

Small-Scale Propellers Operating in the Vortex Ring State

Omkar R. Shetty* and Michael S. Selig†
University of Illinois at Urbana-Champaign, Urbana, IL 61801, USA

The behavior of small-scale propellers operating in vertical descent and through the vortex ring state (VRS) was measured. In particular, a total of 26 propellers with diameters ranging from 9 to 11 in. (0.229 to 0.279 m) were tested in the University of Illinois at Urbana-Champaign (UIUC) 2.8×4 ft (0.853×1.219 m) low-turbulence wind tunnel at low Reynolds numbers to measure the propeller thrust over a range of advance ratios from −0.8 to 0 (rapid descent to hover). Also, time histories of the measured thrust for different propellers were recorded to characterize the unsteady thrust fluctuations for advance ratios through the vortex ring state. The effects of propeller geometry, e.g. pitch and planform effects, on the thrust characteristics of these propellers in the vortex ring state is discussed.

Nomenclature

a = lift-curve slope
AF = activity factor
B = tip loss factor
c = propeller chord length
C_t = rotor coefficient of thrust
C_T = coefficient of thrust
D = propeller diameter
J = advance ratio
n = rotational speed
P_{atm} = atmospheric pressure
q = dynamic pressure
R = propeller radius, ideal gas constant for air
r_c = blade root cutout
T = thrust
T_{air} = air temperature
V = freestream velocity
w = induced velocity
w_h = ideal induced velocity at hover
x = radial station
ρ = air density
σ = propeller solidity, standard deviation
λ = rotor inflow ratio
$\theta_{0.75}$ = propeller twist angle at 75% radial station

*Graduate Student. Department of Aerospace Engineering, Student Member AIAA.
†Associate Professor, Department of Aerospace Engineering, 104 S. Wright St., Senior Member AIAA.
http://www.ae.illinois.edu/m-selig

I. Introduction

The interaction between the induced flow from a propeller (or helicopter rotor) in descent and the freestream velocity acting upward results in the formation of large vortices around the edge of the rotor disk, leading to the vortex ring state (VRS). The VRS condition is observed when the descent velocity is of a similar magnitude as the induced velocity,[1] thereby preventing the vortex rings from convecting away. It is an unsteady, turbulent condition characterized by a loss of collective control and thrust fluctuations. Beyond the VRS, as the descent velocity is increased, the vortices get convected away from the rotor and a definite slipstream is developed. Since the absence of a defined slipstream in the VRS makes it impractical to apply models such as the momentum theory, a considerable amount of research has been conducted to understand the phenomenon in greater detail.

One of the earliest attempts to define the behavior of propellers in descent was undertaken by Glauert[2] who proposed an empirical form of the characteristic curve based on experimental investigation. Castles and Gray[3] later specified an empirical relation between the induced velocity, thrust and vertical descent velocity for rotors in axial descent. They noted the difference in behavior of linearly tapered planforms and rotors with twist as compared with constant chord, untwisted blades. They also observed fluctuations in the force and moment data for the rotors in the VRS. Washizu, et al.[4] investigated and quantified these unsteady aerodynamic characteristics of rotors in the VRS under both axial and inclined descent conditions. They observed the presence of extensive thrust fluctuations in the VRS with a certain periodicity exhibited in some regions of the VRS. Similarly, Yaggy and Mort[5] also examined the fluctuations in thrust under axial and inclined descent for a rigid and flapping propeller, establishing a relation between the extent of these fluctuations and the disk loading. More recently, Betzina[6] studied these phenomena experimentally, noting significant differences in the VRS characteristics of a single rotor and tandem rotor configuration. The possibility of low frequency roll oscillations in tilt-rotor aircraft was also suggested.

Apart from the experimental research, there have been considerable efforts to study the phenomenon computationally. Leishman, et al.[7] carried out a computational study on the onset of the VRS for single and multi-rotor configurations and the flow and rotor geometric factors that affect it. Chen and Prasad[8] developed the ring vortex model to predict the inflow characteristics for rotors in descent.

The current study examines wind tunnel test data obtained from a wide range of small-scale (low Reynolds number) propellers in the VRS and analyzes the results to understand better the effect of propeller parameters such as the pitch, diameter, solidity and the activity factor on the thrust characteristics of propellers in the VRS. For the wind tunnel experiments, a total of 26 propellers were tested and the data analyzed in further sections. The tests were essentially carried out in two stages. The first stage consisted of test runs where steady state thrust coefficient data was acquired as a function of propeller advance ratio. For the second stage of tests, thrust time-history data was recorded for a given advance ratio and the data was analyzed to measure the nature and the extent of thrust fluctuations. This paper discusses the results obtained from the tests.

Testing of small scale propellers in the normal working state has been carried out for several years at the University of Illinois at Urbana-Champaign.[9–11] The existing wind-tunnel setup was modified to enable testing of propellers in axial vertical descent.[12] For the research reported here, the diameters of the propellers tested ranged between 9 and 11 in. (0.229 and 0.279 m). Figure 1 shows the three types of propellers tested for this study, namely the APC Slow Flyer, APC Sport and APC Thin Electric. Table 1 gives the list of the propellers along with the solidity, activity factor and the pitch angle at the 75% radial station. Apart from the specific brand name (APC) and propeller style (Slow Flyer, etc.), the propellers are denoted as $D \times p$ where D is the propeller diameter (in) and p represents the pitch (in/rev) as reported by the manufacturer.

II. Experimental Setup

The tests for this study were conducted at the UIUC subsonic wind tunnel and a detailed description is given in Shetty.[12] The wind tunnel had a cross section of 2.8×4 ft (0.853×1.219 m). An experimental rig was originally designed to test propellers in the normal working state.[9,13] Thrust, torque, and propeller speed (RPM) and the freestream flow speed were measured for the tests using the experimental rig. The propeller thrust was transferred to a load cell mounted on top of the test section by means of a T-shaped structure that pivots about two flexural pivots. The load cell used was an Interface SM-10 with a maximum

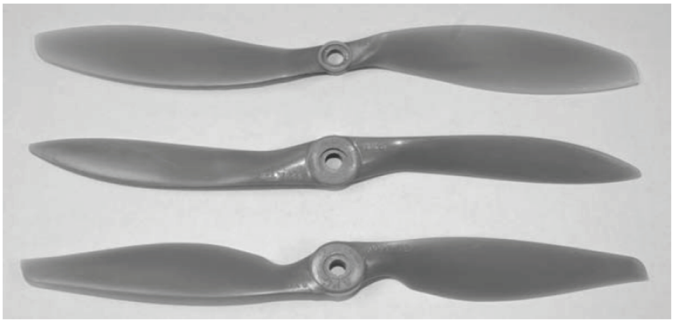

Figure 1. APC Slow Flyer (top), Sport (middle) and Thin Electric (bottom) propellers.

capacity of 10 lb (44.5 N). Figure 2 shows the propeller test setup in the normal working state.

In order to test propellers in descent, the propellers were mounted facing downstream. This caused the thrust to be generated in the opposite direction thereby exerting a compressive force on the load cell. Since the load cell used could withstand only tensile forces, the load cell would be subjected to a constant preloading by means of counterweights, so that at any given time the net force acting on the load cell would be in tension. A Honeywell HOA1180-002 Reflective Sensor was used to measure the RPM of the propeller, and the torque was measured using the RTS-25 and RTS-100 reaction torque transducers. The freestream velocity was measured by a pitot tube connected to a MKS 220DD 1-torr (133.32-N/m^2) transducer. The Astro 020 Planetary System motor and gearbox drove the propellers which with the current configuration could achieve a maximum rotational speed of 7,500 RPM.

From the normal working-state test setup,[9,13] certain changes were made for testing of propellers in axial descent. First, the propeller was turned around and mounted facing downstream to produce thrust in the downstream direction when in VRS. To achieve this operating state, the rotation direction of the propeller was reversed by reversing the polarity of the motor. Second, because of the strong unsteady fluctuations in thrust and torque in the VRS, the torque transducer was removed because it was not designed for such strong unsteady overloading. These modifications can be seen in Fig. 3. Third, the freestream velocity was measured from pressure measurements in the inlet and contraction section of the wind tunnel, instead of the approach described in Brandt[9,13] wherein a pitot probe was position in the test section with the measurements being corrected for the propeller induced flow effects. This change in the method for measuring the freestream was necessary because of the unsteady flow conditions produced by the propeller in VRS. Fourth, correction factors were included in the data acquisition code to account for the solid and wake blockage in VRS.[14,15] Finally, the test parameters measured for the present study were the freestream velocity, propeller speed (RPM) and thrust with the difference being again that no torque measurements were recorded.

Table 1. List of Propellers Tested

Brand	Style	Designation	$\theta_{(0.75R)}$(deg)	Solidity	Activity Factor
APC	Slow Flyer	9×4.7	11.56	0.0978	122.65
		10×4.7	10.27	0.0957	118.34
APC	Sport	9×5	14.87	0.0729	83.97
		10×4	9.93	0.0737	82.81
		10×5	16.60	0.0774	90.37
		10×10	23.97	0.0746	88.12
APC	Thin Electric	9×4.5	12.56	0.0912	98.21
		10×5	13.39	0.0806	83.96
		10×7	16.74	0.0811	84.05
		10×10	24.80	0.0799	81.93

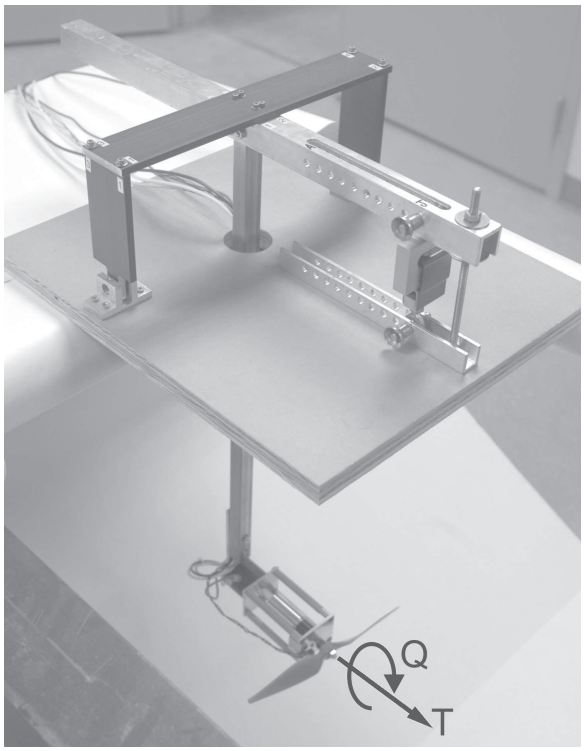

Figure 2. Propeller test apparatus as viewed from above (oriented for measurements in the normal working state, taken from Brandt[9]).

The data acquisition system consisted of a Dell 1.4-GHz Precision-330 computer workstation and a National Instruments™ NI PCI-6031E 16-bit analog-to-digital data acquisition board. The data acquisition software was developed using LabWindows® from National Instruments. For each test run, the propeller was maintained at a constant rotational speed of 4,000 RPM. The freestream velocity was then varied from a value of 8 to 40 ft/sec (2.44 to 12.19 m/s) in increments of 2 ft/sec (0.61 m/s) and the thrust was measured at each condition. Three data points were measured at each condition leading to 51 data points for an entire test run. The data acquisition software determined the air density and freestream velocity from

$$\rho = \frac{P_{atm}}{R\,T_{air}} \tag{1}$$

$$V = \sqrt{\frac{2q}{\rho}} \tag{2}$$

The advance ratio J and the thrust coefficient C_T are defined as

$$J = \frac{V}{nD} \tag{3}$$

$$C_T = \frac{T}{\rho\, n^2 D^4} \tag{4}$$

Based on propeller geometry and the thrust, the induced velocity and the net inflow were calculated using the Eqs. 5–7. The values for the tip loss factor (B) and the blade root cutout (r_c) were taken as 0.97 and 0.15 respectively. The thrust coefficient and the freestream velocity data were obtained from the wind tunnel experiments, while the pitch angle at the 75% station ($\theta_{0.75}$) and the propeller solidity (σ) was taken from the propeller geometry measurements. Based on these parameters, the rotor inflow ratio (λ) was calculated using Eq. 5. From the value of the inflow ratio, the induced velocity (w) was calculated using

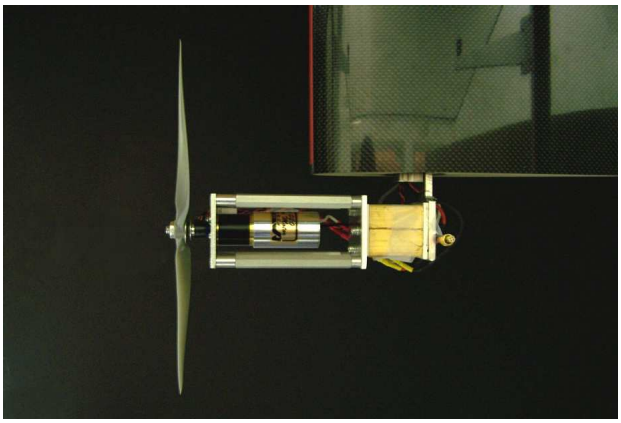

Figure 3. Modified test apparatus for propellers in descent (freestream flow from left-to-right while thrust is directed downstream).

Eq. 6. The ideal induced velocity at hover (w_h) was calculated using Eq. 7. From these set of equations, the non-dimensionalized induced velocity (w/w_h) and the net inflow ($(V + w)/w_h$) were calculated using the relations:

$$\frac{3}{2}(B^2 - r_c^2)\lambda = -\frac{6C_t}{\sigma a} + \theta_{0.75}(B^3 - r_c^3) \tag{5}$$

$$w = \lambda(2\pi n)\frac{D}{2} - V \tag{6}$$

$$w_h = \sqrt{\frac{T}{2\rho A}} \tag{7}$$

Along with the complete test runs, the thrust time-history data was also recorded. The signal was low pass filtered at 10 Hz by a Butterworth filter present in the signal conditioner. The data was recorded for 90 sec at a sampling frequency at 120 Hz at 9 different advance ratios. The time-history tests were conducted for 10 propellers in all.

III. Results

Figure 4 shows the plot for the coefficient of thrust as a function of the advance ratio for the APC Thin Electric 10×5. According to convention, as the propeller is tested under descent conditions, the velocity and hence the advance ratio is represented on the negative axis and the thrust (and hence the C_T) on the positive axis. It is observed that as the velocity increases, C_T decreases until it reaches a minimum value. Beyond this condition, the C_T increases as the descent velocity increases. Based on the blade element theory,[16] the induced velocity and the total inflow of the propeller are calculated. Figures 5 and 6 show the induced velocity and the net inflow as a function of the non-dimensionalized freestream velocity.

The plots represent the transition, starting from the hover condition through the turbulent working state and finally for the most cases culminating at the windmill state. The thrust coefficient represented as a function of advance ratio clearly illustrates the loss in thrust experienced in the VRS. This trend is similar to results obtained in comparative studies. Similar data were collected for all the propellers tested.

The data is analyzed with respect to the geometric characteristics of the propellers, namely the propeller pitch and the activity factor. The thrust time history data is analyzed and the plots are created that compare the thrust fluctuations experienced in the VRS.

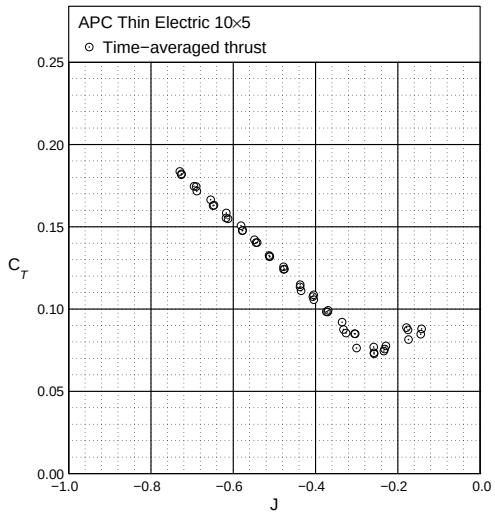

Figure 4. Time-averaged thrust characteristics for the APC Thin Electric 10×5.

A. Pitch Comparison

Figure 7 shows the thrust characteristics for APC Thin Electric propellers of diameter 10 in.(0.254 m). The propellers tested for this set of data are the Thin Electric 10×5, Thin Electric 10×7 and the Thin Electric 10×10 propellers. The pitch in this case is varied between 5 in/rev to 10 in/rev (0.127 m/rev to 0.254 m/rev). The blade pitch angle at the 75% radial station given in degrees increases correspondingly from 13.39 deg to about 19 deg with an increase in the pitch. It can be seen that as the pitch increases, the minimum C_T is achieved at a higher descent velocity and thus at a lower (more negative) advance ratio. Also, the minimum value of C_T increases with an increase in the blade angle at the 75% station. These findings seem to be in agreement with the trends observed in the data, presented by Washizu, et al.[4]. The results of a similar study carried out for APC Sport propellers of diameter 10 in (0.254 m) are shown in Fig. 8. The propellers tested here are the Sport 10×4, Sport 10×5 and the Sport 10×10 propellers. The data exhibit a similar trend as that of the Thin Electric in Fig. 7. It is observed that for propellers with higher values of pitch, the value of C_T displays very little variation, remaining nearly constant up to a certain value of J, beyond which the C_T increases with an increase in the advance ratio as for the other cases.

It might seem suggestive based on this trend that increasing the pitch of the propeller would be a solution to avoid the drop in the thrust experienced in the VRS. However the data plotted is the time-averaged data and does not take the instability and hence the thrust fluctuations into consideration.

B. Planform Comparison

The next set of tests focused on the effect of the propeller planform on the thrust characteristics in the VRS. For the purpose of these tests, the data from three propellers are compared, each having an identical diameter and pitch but with a different planform. The three types of propellers vary quite significantly as far as the construction of the propeller is concerned. Both the APC Sport and Thin Electric propellers have thicker airfoil sections and rounder leading edges as compared with the Slow Flyer propellers which have a sharper leading edge and thinner airfoil section. This difference in the propeller geometry leads to a greater amplitude of tip vibration observed for the Slow Flyers in general while testing in the VRS. The propellers also exhibit a difference in the chord distribution. Typically, the Slow Flyers and Thin Electric propellers have a thicker chord distribution along the radial stations. This difference in the chord distribution of the

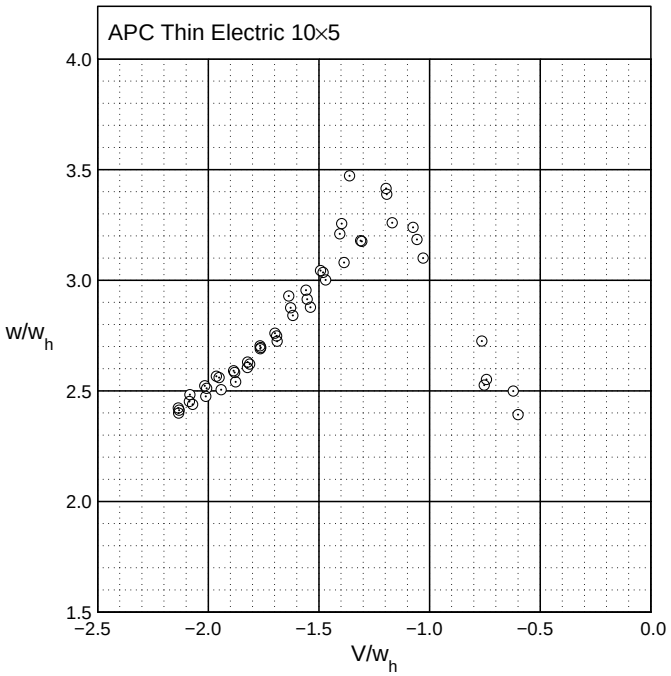

Figure 5. Induced velocity for the APC Thin Electric 10×5.

propellers is compared using the activity factor, which is calculated using the following equation:

$$AF = \frac{10^5}{16} \int_{0.15R}^{1.0R} (\frac{c}{D}) x^3 dx \tag{8}$$

Figure 9 compares the APC Slow Flyer, Sport and Thin Electric 9 in. (0.229 m) diameter propellers having a pitch of approximately 5 in/rev (0.127 m/rev). From this figure, it is observed that, although all three propellers attain the minimum value of C_T at a similar value of J, the rate at which C_T increases with respect to the advance ratio beyond the point of minimum thrust varies distinctly for each of the three propellers. The Slow Flyer shows a maximum value of the slope while the Sport propeller exhibits the minimum. It is likely that this behavior is a direct function of the activity factor of the propeller. Among the propellers in Fig. 9, the APC Slow Flyer (AF = 122.65) has the highest value of Activity Factor, followed by the Thin Electric (AF = 98.21) and the Sport (AF = 83.97) has the least value. Similarly Fig. 10 gives a comparison of three APC propellers with a diameter of 10 in. and a pitch of approximately 5 in/rev. Again the Slow Flyer 10×4.7 (AF = 118.34) shows the highest thrust slope beyond the minimum thrust point. However, in this case the Sport 10×5 (AF = 90.37) has a higher slope than the Thin Electric 10×5 (AF = 83.96).

Figures 9–10 reveal a strong dependence of the thrust characteristics of the propeller on the value of the activity factor. It is concluded based on these plots that the higher the activity factor of the propeller, the higher is the rate at which the thrust increases as a function of the advance ratio and the easier it becomes to recover from the VRS. This is understandable as a higher value of the activity factor implies a thicker chord distribution, thereby leading to a greater value of the generated thrust.

C. Thrust Fluctuations

For the final set of tests, the thrust time history data was recorded and analyzed. As is expected, the thrust data is relatively steady for the static test (hover condition). As the descent velocity increases, the extent of the fluctuations increases until the point of minimum thrust is achieved. The maximum fluctuations are observed at this advance ratio to the order of approximately ±30%. Beyond this point, the extent of the fluctuations decreases with an increase in descent velocity. Figure 11 shows this trend for the APC

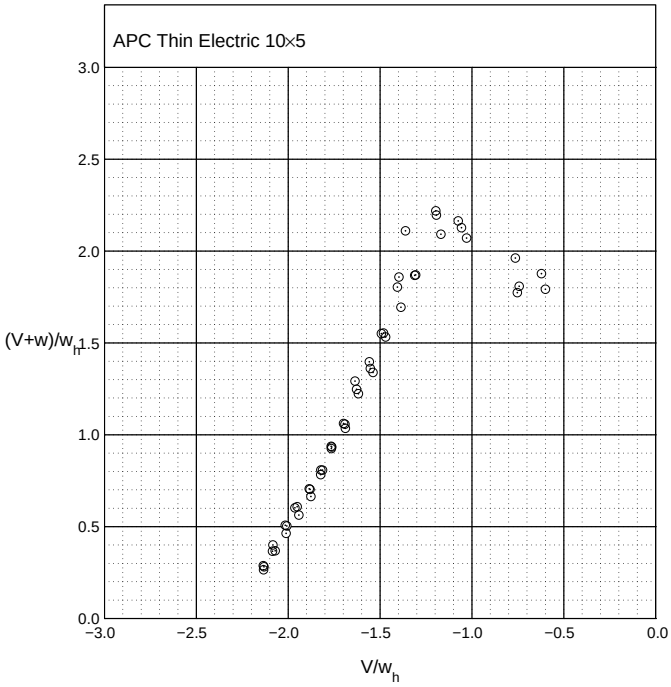

Figure 6. Net inflow for the APC Thin Electric 10×5.

Thin Electric 10×5. Here the extent of the fluctuations are represented by the actual measured limits and variations of $\pm 3\sigma$ where σ is the standard deviation. Comparing the fluctuating thrust coefficient data for propellers with a similar planform and varying pitch, it is observed that the magnitude of thrust fluctuations increases with an increase in the propeller pitch. Figures 11–13 exhibit this trend for the APC 10 in. (0.254 m) Thin Electric propellers.

This trend is similar to that observed from the data presented by Yaggy and Mort.[5] Figures 14–16 represent the time histories of the thrust coefficient for the APC Thin Electric 10×5 at different advance ratios over a period of 5 sec. The time history data was acquired for a total of 10 propellers.[12]

IV. Conclusion

The results of these tests do show specific trends that could lead to a better understanding of the vortex ring state for propellers as low Reynolds numbers. Some of these conclusions are:

- The reduction in thrust experienced by propellers in descent is highly dependent on the pitch of the propeller. The advance ratio at which the minimum thrust is observed, reduces with an increase in pitch. Also, the extent of the reduction in the thrust reduces as the pitch increases.
- The thrust characteristics of a propeller in descent also depend on the propeller activity factor. An increase in the activity factor causes a steeper increase in the C_T beyond the point of minimum thrust.
- An analysis of the propeller thrust time history reveals a variation in the extent of thrust fluctuations as the advance ratio is varied, with maximum fluctuations of a magnitude of approximately $\pm 30\%$ observed at the advance ratio corresponding to the minimum thrust. Also, the magnitude of the fluctuations is dependent on the propeller pitch as well. Propellers with a higher pitch exhibit greater thrust fluctuations, and these fluctuations occur over a greater range of advance ratios.

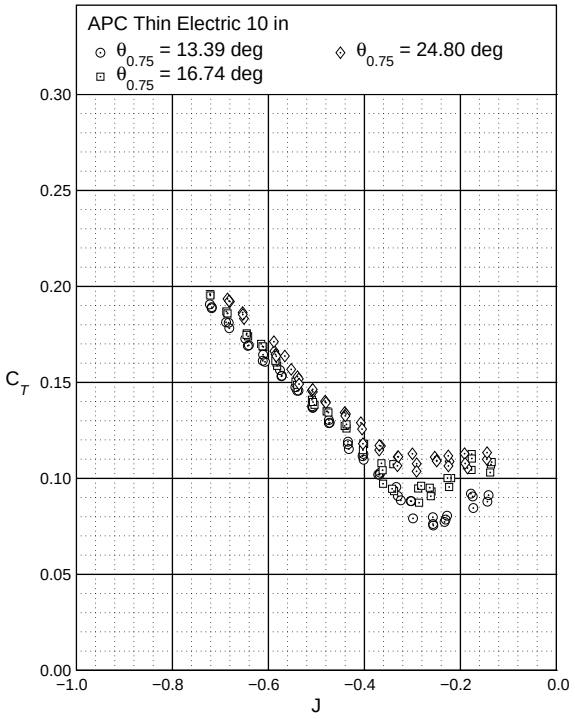

Figure 7. Thrust characteristics for three APC Thin Electric propellers with a diameter of 10 in. (Thin Electric 10×5, 10×7 and 10×10 propellers).

References

[1]Bramwell, A. R. S., *Helicopter Dynamics*, John Wiley and Sons, New York, 1976.

[2]Glauert, H., "The Analysis of Experimental Results in the Windmill Brake and Vortex Ring States of an Airscrew," Aeronautical Research Council R&M 1026, 1926.

[3]Castles, W. and Gray, R., "Empirical Relation between Induced Velocity, Thrust and Rate of Descent of a Helicopter as Determined by Wind-Tunnel Tests on Four Model Rotors," NACA TN 2474, 1951.

[4]Washizu, K., Azuma, A., Koo, J., and Oka, T., "Experiments on a Model Helicopter Rotor Operating in the Vortex Ring State," *Journal of Aircraft*, Vol. 3, No. 3, 1966, pp. 225–230.

[5]Yaggy, P. and Mort, K., "Wind-Tunnel Tests of Two VTOL Propellers in Descent," NACA TN D-1766, 1963.

[6]Betzina, M. D., "Tiltrotor Descent Aerodynamics: A Small-Scale Experimental Investigation of Vortex Ring State," American Helicopter Society 57th Annual Forum, Washington, D. C., May 2001.

[7]Leishman, J. G., Bhagwat, M. J., and Ananthan, S., "Free-Vortex Wake Predictions of the Vortex Ring State for Single-Rotor and Multi-Rotor Configurations," American Helicopter Society 58th Annual Forum, Montreal, Canada, June 2002.

[8]Chen, C. and Prasad, J. V. R., "Simplified Rotor Inflow Model for Descent Flight," *Journal of Aircraft*, Vol. 44, No. 3, 2007, pp. 936–944.

[9]Brandt, J. B., *Small-Scale Propeller Performance at Low Speeds*, Master's thesis, University of Illinois at Urbana-Champaign, Department of Aerospace Engineering, 2005.

[10]Tehrani, K., *Propellers in Yawed Flow at Low Speeds*, Master's thesis, University of Illinois at Urbana-Champaign, Department of Aerospace Engineering, 2006.

[11]Uhlig, D. V., *Post Stall Behavior at Low Reynolds Numbers*, Master's thesis, University of Illinois at Urbana-Champaign, Department of Aerospace Engineering, 2007.

[12]Shetty, O., *Measurements of Small-Scale Propellers Operating in the Vortex Ring State*, Master's thesis, University of Illinois at Urbana-Champaign, Department of Aerospace Engineering, 2010.

[13]Brandt, J. B. and Selig, M. S., "Propeller Performance Data at Low Reynolds Numbers," Aiaa paper, January 2011.

[14]Barlow, J. B., W. H. Rae, Jr., and Pope, A., *Low-Speed Wind Tunnel Testing, Third Ed.*, John Wiley and Sons, New York, 1999.

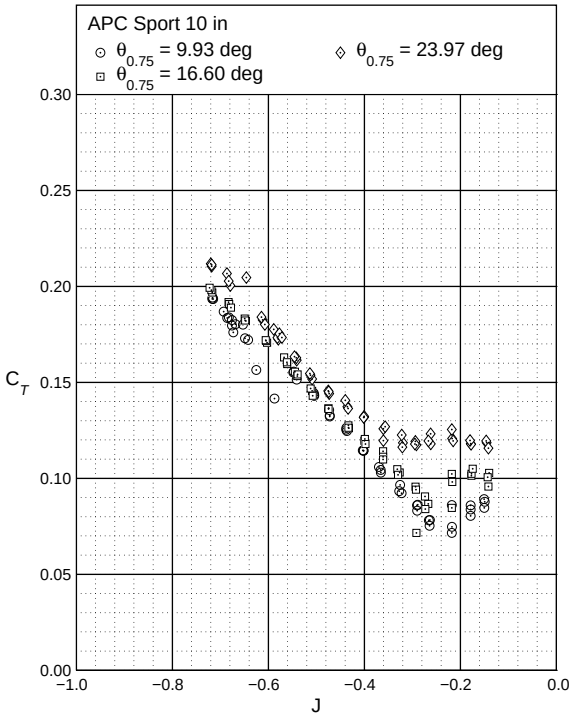

Figure 8. Thrust characteristics for three APC Sport propellers each with a diameter of 10 in. (Sport 10×4, 10×5 and 10×10 propellers).

[15]Maskell, E. C., "A Theory of the Blockage Effects on Bluff Bodies and Stalled Wings in a Closed Wind Tunnel," Reports and Memoranda 3400, 1963.

[16]Johnson, W., "Model for Vortex Ring State Influence on Rotorcraft Flight Dynamics," NASA TP-2005-213477, December 2005.

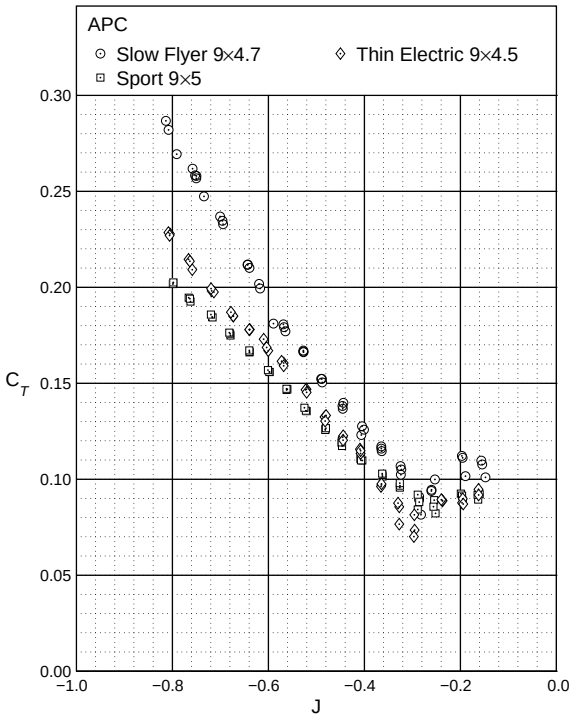

Figure 9. Thrust characteristics for the APC Slow Flyer, Sport and Thin Electric propellers each with a diameter of 9 in. and similar pitch.

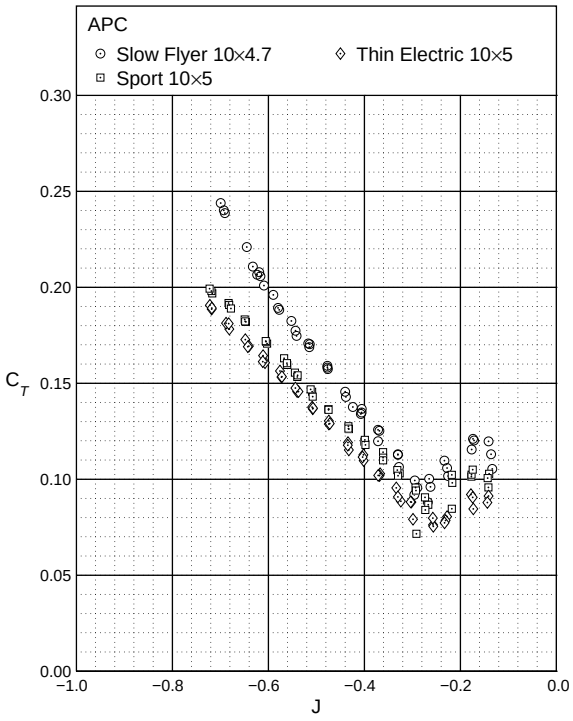

Figure 10. Thrust characteristics for the APC Slow Flyer, Sport and Thin Electric propellers each with a diameter of 10 in. and similar pitch.

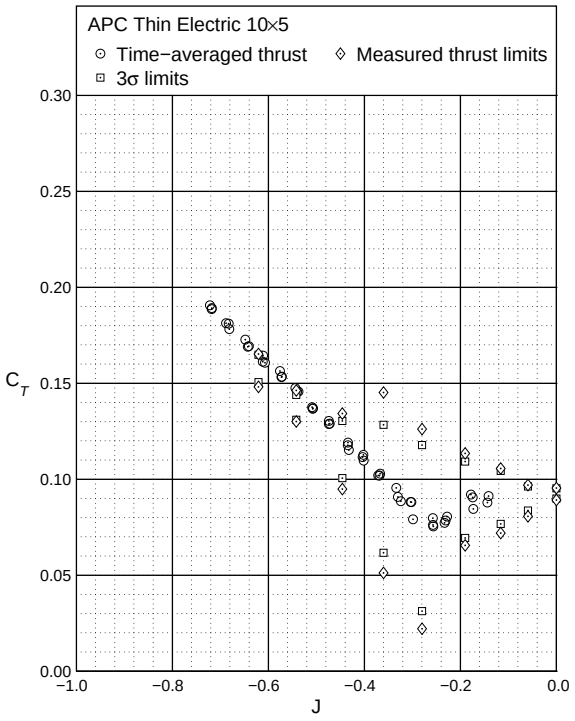

Figure 11. Time-averaged and fluctuating thrust coefficient for the APC Thin Electric 10×5.

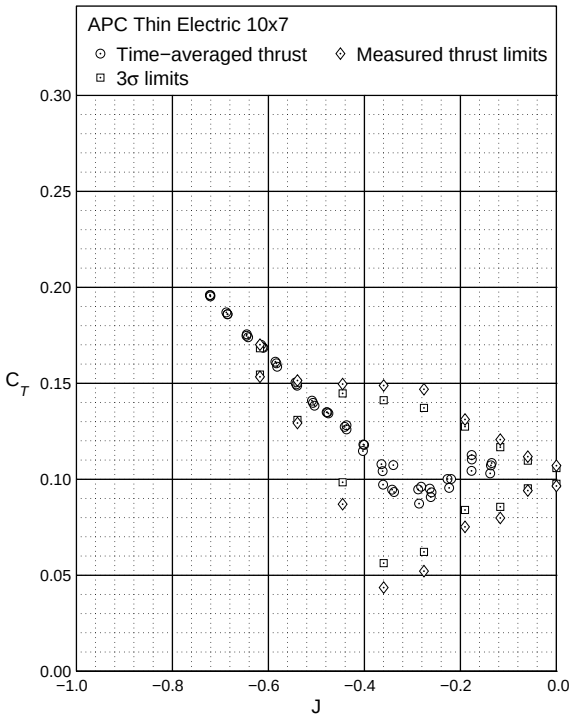

Figure 12. Time-averaged and fluctuating thrust coefficient for the APC Thin Electric 10×7.

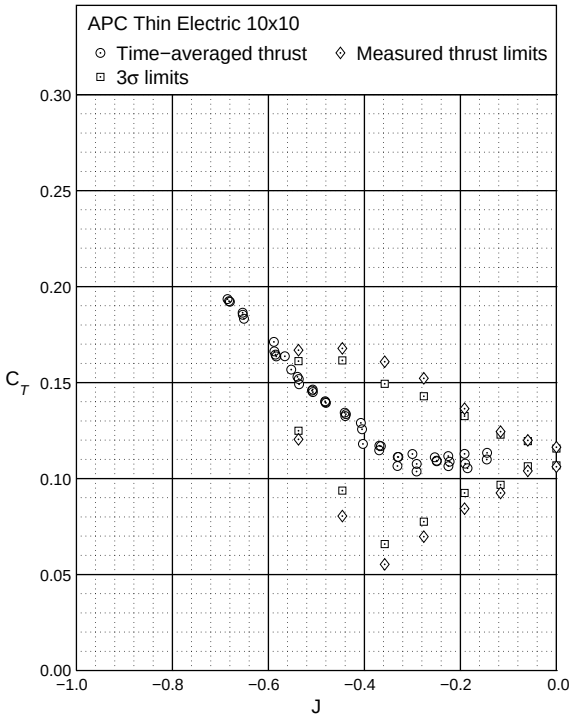

Figure 13. Time-averaged and fluctuating thrust coefficient for the APC Thin Electric 10×10.

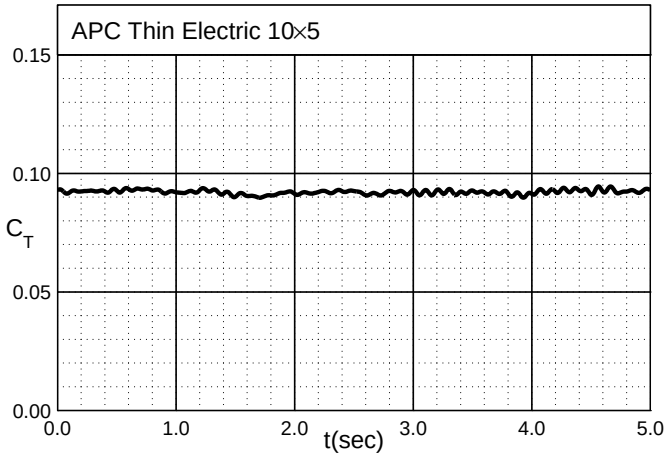

Figure 14. Thrust coefficient time history for the APC Thin Electric 10×5 in hover.

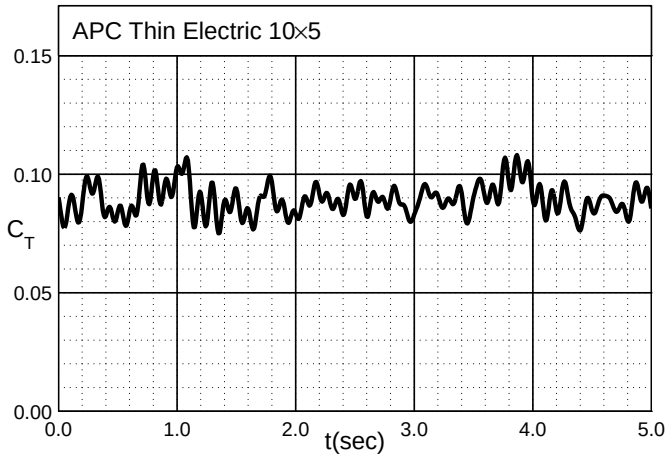

Figure 15. Thrust coefficient time history for the APC Thin Electric 10×5 at $J = -0.19$.

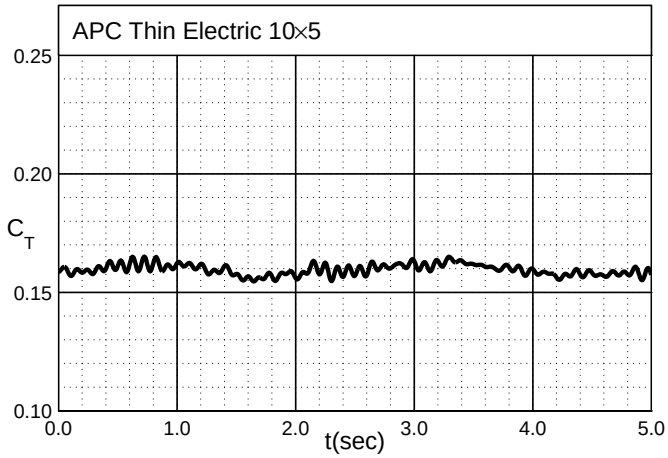

Figure 16. Thrust coefficient time history for the APC Thin Electric 10×5 at $J = -0.62$.